Determination of the Aerodynamic Characteristics of Low Reynolds Number Flows over Small Uninhabited Aerial Vehicles

Authors:
Hugo T. C. Pedro
Dr. Marcelo H. Kobayashi (advisor)

Motivation

The interest in small-unmanned aerial vehicles (UAV's) has increased greatly in the past decade. The size of such vehicles and the velocity at which they operate results in low Reynolds (Re) number flight regime, in the 15000 − 500000 range. The high Re aerodynamics is well established, however the same cannot be said for the low Re regime. In this range the wing's aerodynamic performance can deteriorate rapidly as the Re number decreases. To simply scale the vehicle to a smaller size is not the solution. Further research in this range of Re numbers is necessary. Recently was reported that the humpback whale flipper is optimized to prevent stall and to improve aerodynamic performance. These features allow these animals to be extremely mobile with great turning ability, which is necessary to catch prey. This observation together with the fact that the Reynolds number for the humpback whale falls in the aforementioned low Re range propelled the experimental study the humpback whale flipper. The flippers for this species display a very characteristic scalloped leading edge, whereas the flippers of other species less maneuverable are much smoother. The experiments compared a flipper with tubercles with a smooth flipper. The researchers reported an improvement in the aerodynamic performance as well an increase in the angle of attack at which the flipper stalls. However no flow visualization was performed, therefore the reasons why the scalloped flipper performs better were not uncovered. In this work we performed the numerical simulation of the setup used for the experimental study. The unsteady turbulent flow field for the scalloped flipper and for the smooth flipper was accurately determined which produced detailed information necessary to fully understand the mechanism behind the reported improvement.

Our goal with this work is to increase the knowledge about these lower Re number flows, which will be useful for the design of more efficient UAV's wings.

Methods

The flow around the flipper was modeled as incompressible at a Re number, based on the mean flipper chord, of 50 000. The numerical simulations were preformed with the commercial software package Fluent. The turbulent flow was solved using the DES (Detached Eddy Simulation) formulation. The numerical simulation used the segregated SIMPLE solver with a second order accurate spatial discretization. The time integration is performed with an implicit second order scheme.

The simulations model the flipper and the wind tunnel test-section walls. Both flippers are 56.25 cm long and have a projected plan-form area of 715 cm^2, which yields a mean chord of 12.7 cm. Reynolds number for the experiments was in the range 5.0e5 — 5.2e5. To maintain this value in our numerical simulation the velocity at the inflow boundary is 60 ms^{-1}, which corresponds to a Mach number of 0.18.

A steady RANS calculation was used as the starting point for the unsteady calculations. This flow field was then used as the initial condition for the time-dependent solution.

Use of HPC resources

The simulation was performed with the commercial code FLUENT available at the MHPCC Tempest IBM P4 machines. There was no need for code compilation. The code is parallelized, and all runs were done using 32 processors on a single node. The meshes had 2.6 million nodes in average, which required several gigabytes of RAM memory. Numerical stability constrains required a time step of 0.0001 seconds, and 2500 time steps were calculated which corresponds to 0.25 seconds of simulation. A job with these characteristics required 20 to 24 hours to complete, and generated about 50 GB of data.

The interactive nodes were also used to post-process the data.

Results

A. Comparison With Experiment

Figure 1 depicts the results for both flippers. The numeric simulations were concentrated in the range of 12 - 18 angle of attack since the experiments determined this as the range were the different geometries showed the most noticeable differences. They show a very good agreement with their experimental counterpart.

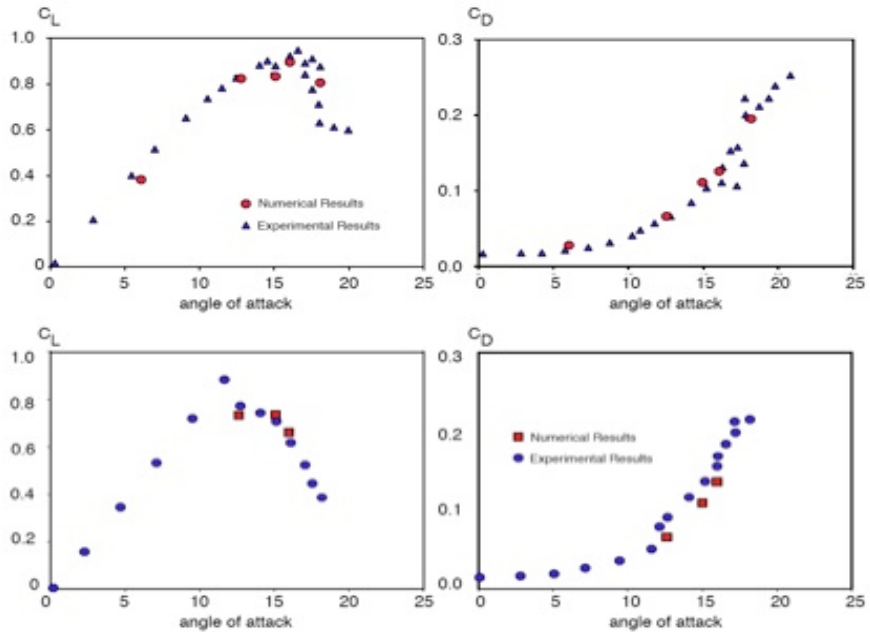

Figure 0: Force coefficients CL and CD as a function of the angle of attack for the scalloped flipper (top) and smooth flipper (bottom). Comparison between experimental and numerical results.

B. Vorticity field

One of the most important questions we want to clarify is whether or not the leading-edge tubercles in the scalloped flipper work as vortex generators. The basic

principle of those devices is to generate stream-wise vortices, hence the analysis of vorticity at the flipper surface is of prime importance. In figure 2 it is depicted an isosurface of vorticity magnitude. The value is the same for both figures (a) and (b).

The figure shows that at the root and the tip both flippers produce similar vortical structures. Has one could expect the most noticeable stream-wise vortex at these locations is the tip vortex. The outboard 1/5 as well as the root of both wings are covered by large vortical structures, which seem somewhat chaotic. Indeed, as we shall demonstrate ahead in these regions the flow is separated giving rise to chaotic flow motion. In the flipper midsection that similarity completely vanishes. Instead, we observe that the scalloped flipper displays large stream-wise vortices aligned with the tubercles. On the other hand the smooth flipper shows no such structures. The high values of vorticity over the midsection of the scalloped flipper locate the center of rotation of the stream-wise vortices. These eddies re-energize the boundary layer by carrying high momentum flow close to the wall.

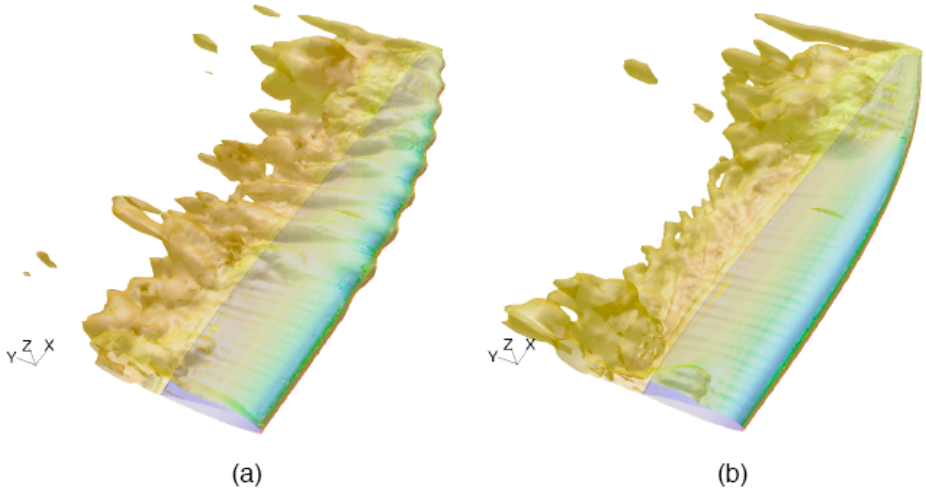

Figure 2: Instantaneous vorticity magnitude isosurface colored by pressure for = 15°. (a) Scalloped flipper, (b) smooth flipper.

C. Separation

Due to the large span-wise variations of the flipper's chord we can identify two different regions in terms of the Reynolds number. The average Reynolds number for the outboard third of the flipper is clearly a low Reynolds number (< 200000), whereas the inboard section's Re falls in the category of high Reynolds numbers (> 500000). The separation is studied by investigating the shear stress at the flipper's surface. In figure 3 and 4 the averaged shear stress streak-lines at the flipper surface are displayed. When the streak-lines point in the flow direction the flow is attached whereas the reversed indicates flow separation and the line to which the streak-lines are attracted represents the separation line. These figures clearly show that the two aforementioned regions display completely different types of separation. In the outboard section the flow separates in the leading edge whereas in the inboard section we observe a trailing edge type of flow separation. This characteristic is common to both flipper geometries. This type of separation can be very damaging for the flipper performance since the separated region can grow very fast in the root direction. Indeed, the smooth flipper displays that behavior.

The increase of the angle of attack from 12.5 to 15 degrees propagates the separation region rapidly towards the flipper's root. As we saw previously in the aerodynamic forces plots this damages the aerodynamic performance greatly by decreasing C_L sharply and increasing C_D. As for the scalloped flipper, we observe that the separated region for α = 12.5° is comparable to that of the smooth flipper, however in this case the change in the angle of attack did not increase the separation so dramatically. This behavior resembles another passive separation control that can be found in real aircrafts: the wing fence. These devices create a physical barrier to the span-wise motion, which prevents the separation growth from the tip to the root of the wing.

These figures also demonstrate that the scalloped flipper resists to separation more efficiently than the smooth flipper in the high Reynolds region, as well. Once again the explanation is based on the presence of the stream-wise vortices that energize the trailing portion of the flipper delaying separation.

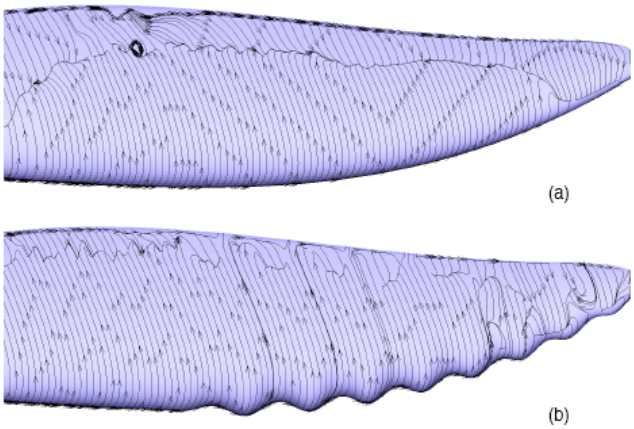

Figure 3: Averaged shear stress streak-lines for α = 12.5°. (a) Smooth flipper, (b) scalloped flipper.

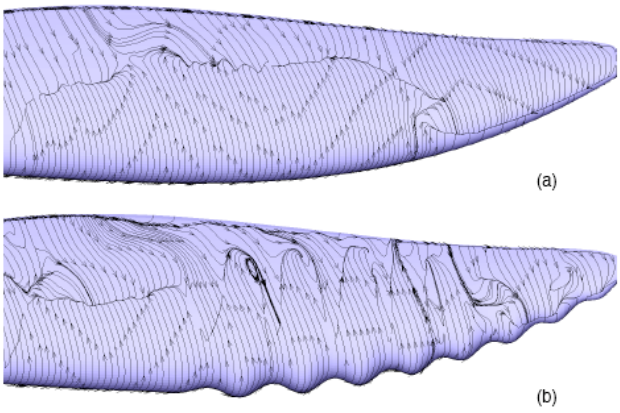

Figure 4: Averaged shear stress streak-lines for α = 15°. (a) Smooth flipper, (b) scalloped flipper.

Acknowledgements

Funding was provided by the University of Hawaii through a MHPCC Student Engagement Grant. HPC resources were provided by MHPCC.

References

D. S. Miklosovic, M. M. Murray, L. E. H. and Fish, F. E., *"Leading-edge tubercles delay stall on humpback whale (Megaptera novaeangliae) flippers"*, Physics of Fluids, Vol. 16, 2004, pp. 39 – 42.

Becky L. Woodward, J. P. W. and Fish, F. E., *"Morphological Specializations of Baleen Whales Associated With Hydrodynamic Performance and Ecological Niche"*, Journal of morphology, Vol. 267, 2006, pp. 1284 – 1294.

Pedro, Hugo T. C. and Kobayashi, Marcelo H., *"Numerical Study of stall delay on humpback whale flippers"*, paper 2008-0584, 46th AIAA Aerospace Sciences Meeting and Exhibit, 7-10 January 2008, Reno, Nevada.